Hybrid-PIC Simulation on Plasma Flow of Hollow Cathode

IEPC-2015-15／ISTS-2015-b-15

Presented at Joint Conference of 30th International Symposium on Space Technology and Science
34th International Electric Propulsion Conference and 6th Nano-satellite Symposium,
Hyogo-Kobe, Japan
July 4 – 10, 2015

K. Kubota[1]
Japan Aerospace Exploration Agency, Chofu, Tokyo, 182-8522, Japan

Y. Oshio[2]
Japan Aerospace Exploration Agency, Sagamihara, Kanagawa, 252-5210, Japan

H. Watanabe[3]
Tokyo Metropolitan University, Hino, Tokyo, 191-0065, Japan

S. Cho[4] and Y. Ohkawa[5]
Japan Aerospace Exploration Agency, Chofu, Tokyo, 182-8522, Japan

and

I. Funaki[6]
Japan Aerospace Exploration Agency, Sagamihara, Kanagawa, 252-5210, Japan

Abstract: In order to understand plasma properties of hollow cathodes, a numerical simulation code with Hybrid-PIC model has been developed, in which ions and electrons are modeled as particles and fluid, respectively. In this study, as a first step, the applicability of the model is demonstrated, and then the influences of the insert temperature on the flow field are discussed for a discharge current of 30 A and a mass flow rate of 1 mg/s. The electron density for the maximum insert temperature of 1900 K agrees well with the experimental data of JPL. The results also show that the electron density tends to be higher with lower insert temperature due to the higher electron temperature inside the cathode tube. The higher electron temperature is caused by the energy loss suppression resulting from the higher sheath voltage on the insert surface. It was also found that charge exchange collisions make the location of the electron density peak shifted upstream.

Nomenclature

A	=	Richardson-Dushman coefficient
e	=	elementary charge
$\boldsymbol{E}$	=	electric field
j	=	current density
k	=	Boltzmann constant

[1] Researcher, Aeronautical Technology Directorate, kubota.kenichi@jaxa.jp
[2] Project Researcher, Institute of Space and Astronautical Science, oshio.yuya@jaxa.jp
[3] Assistant Professor, Faculty of System Design, hwatanabe@tmu.ac.jp
[4] Researcher, Aeronautical Technology Directorate, choh.shinatora@jaxa.jp
[5] Associate Senior Research Engineer, Research and Development Directorate, okawa.yasushi@jaxa.jp
[6] Associate Professor, Institute of Space and Astronautical Science, funaki.ikkoh@jaxa.jp.

L	=	characteristic length
n	=	number density
m	=	mass of particle
p	=	pressure
T	=	temperature
$\boldsymbol{u}$	=	velocity
μ	=	mobility
ν	=	collision frequency
ϕ	=	electric potential
Subscripts		
c	=	cathode (insert) surface
e	=	electron
em	=	emitter
i	=	ion
sh	=	sheath
w	=	work function

I. Introduction

Recent years, research and development of high power Hall thrusters have been activated to apply them to all-electric satellites and/or deep-space explorers. To shorten trip time, a thrust of several hundred mN should be attained, which leads to requirement of a cathode which can provide electron current about several tens of amperes or more.

A number of experimental and numerical efforts on high-current hollow cathodes have been made for years by researchers,[1-4] and overall characteristics of hollow cathode plasma are being unveiled. One of the most informative works will be the plasma-diagnosis data along the centerline obtained by the fast-scanning probe developed at JPL,[1] and numerical simulations by OrCa2D which utilize the fluid approximation for all species.[2] According to the experimental results obtained at JPL,[5] effective electron emission, which is preferable especially for high-current situations, could be achieved by using a large-diameter orifice; then the plasma tends to extend along the insert and have a peak well inside the insert region. This policy makes the gas density rarefied not only inside the cathode but also around the orifice region, which leads to requirement of careful treatment with regard to rarefied effect. In terms of lifetime of cathodes, sputtering of a keeper electrode by energized ions has been serious issue.[6] One of the most probable origins of the high-energy ions is the ion acoustic turbulence (IAT), where electron energies are transferred to the propagating ion acoustic wave via inverse electron Landau damping, and then the energy are dissipated via collisional ion damping.[7] In order to capture such processes, kinetics of ions should be pursued at least.

Developing a high current hollow cathode, we believe numerical simulations as well as experiments are quite beneficial to understand substantial physics in cathodes and optimize working conditions. To take the rarefied effect and ion kinetics into account in a natural way, we are developing a numerical code with a Hybrid-PIC (Particle In Cell) model, in which heavy particles (neutrals and ions) and electrons are modeled as particles and fluid, respectively. The objectives of this study are to demonstrate the applicability of Hybrid-PIC model for the hollow cathode simulation as a first step. The flow properties and influences of the insert temperature on the flow field are discussed under the condition of a constant discharge current and a constant mass flow rate. The electron density profiles are compared to the experimental data to validate our results. The role of CEX collisions in the electron density profile is also discussed.

II. Numerical Modeling

A. Hybrid-PIC Model

The flow was assumed to be axisymmetric and quasi-neutral in the bulk region. The kinetics of ions was traced with PIC method and collisions were dealt with DSMC (Direct Simulation Monte Carlo) method, where charge exchange collision (CEX) and elastic collisions (n-n, n-i, i-i) were taken into account. Ionization process takes place by electron impact on neutrals, whereas multiply charged ions were ignored. Since the neutral density is quite higher than the ion density, a typical weight of a macroneutral was set much larger than that of a macroion. Thus the mass decay model for neutrals was used to implement the ionization process.[8] CEX is often modeled as "identity switch" between a neutral and an ion without further interaction, but such a model neglects interaction via the polarization potential which can lead to a large scattering angle. In this study, CEX and elastic collision were implemented with the united theory proposed by Nanbu,[9] in which the interaction through the polarization potential is simply modeled in a stochastic way. The model includes two free parameters: cut-off dimensionless impact parameter and a coefficient to determine a maximum impact parameter effective for CEX. In this study, the former was assumed to be 9 as proposed in the original literature. As to the latter parameter, Nanbu determined it for He, Ne, Ar, and Kr so that the drift velocity resulting from the model agrees with the experimental data. The resultant values are 2.6 for He, Ne, Ar, and 2.5 for Kr. Since the value for Xe is not available, we assumed the same value as Kr.

The electrons were modeled by the drift-diffusion model.

$$\boldsymbol{u}_e = -\mu_e \boldsymbol{E} - \frac{\mu_e}{e}\frac{\nabla p_e}{n_e}, \quad \boldsymbol{E} = -\nabla\phi \tag{1}$$

The electron number density is equal to the ion number density determined by ion PIC due to the quasi-neutral assumption. In the calculation of the electron mobility, the effect of anomalous resistivity due to IAT was included .[10]

$$\mu_e = \frac{e}{m_e \nu_e}, \quad \nu_e = \nu_{en} + \nu_{ei} + \nu_a, \quad \nu_a = \alpha\omega_{p,i}\frac{|\boldsymbol{u}_e|}{c_i} \tag{2}$$

The factor of T_e/T_i appeared in the original formula of ν_a was assumed to be included in the coefficient α in accordance with Ref. 10. In all results shown here, α was empirically set at 0.001. By substituting Eq. (1) into the current conservation law, we obtain the elliptic differential equation to determine the electric potential.

$$\nabla\cdot en_e(\boldsymbol{u}_i - \boldsymbol{u}_e) = 0 \;\rightarrow\; \nabla\cdot n_e\mu_e\nabla\phi = \nabla\cdot\left(n_e\boldsymbol{u}_i + \frac{\mu_e}{e}\nabla p_e\right) \tag{3}$$

The electron temperature is given from the steady-state energy conservation equation,

$$\nabla\cdot\left(\frac{5}{2}n_e k T_e \boldsymbol{u}_e + \boldsymbol{q}_e\right) = \boldsymbol{j}_e\cdot\boldsymbol{E} - Q_{ion} - Q_{exc} \tag{4}$$

where Q_{ion} and Q_{exc} represent energy consumption due to ionization and excitation, respectively.[11] Equations (3) and (4) were discretized with finite element methods and were solved by means of a direct solver to enhance numerical stability. As a system solver, we utilized the parallelized sparse direct solver called MUMPS.[12] The solver to trace particle dynamics is also parallelized by means of domain decomposition, where the computational domain is dynamically decomposed to make a load factor of each process uniform.

B. Computation Target

Since we have not obtained our own experimental data of high-current cathode, we assumed imaginary cathode as the simulation target. The inner diameter and the axial length of the insert, however, were set to be the same values as those of 1.5 cm-class cathode of JPL.[13] Since its plasma parameters had been closely investigated in the wide operating range, we can utilize them to validate the simulation results.

C. Boundary Conditions

At the inlet boundary, the working gas is fed uniformly as neutrals and has an assumed temperature of 500 K. Once an ion collides with the wall, it is recombined with an electron and reflected as a neutral. Then some macroions are merged so as to create one macroneutral due to the weight disparity. We can freely set an accommodation factor to specify the degree of thermalization to the wall temperature, but the results shown here assumed an accommodation factor as unity, i.e. the particles are completely thermalized to the wall temperature. On the wall boundaries, the ion/electron density is modified so as to satisfy the Bohm condition. On the insert surface, the temperature profile was assumed to be the measured one obtained by JPL.[10] With the fitted curve of the normalized profile shown in Fig. 1, the maximum temperature is parametrically varied as mentioned later. On the plume boundaries, while the neutrals penetrate the boundary, the ions are reflected. This is because, according to the plasma diagnosis, the further apart from the cathode orifice, the higher the electric potential become.[14] When the ion density becomes lower than a lower limit value on the plume boundary, macroions are supplemented so as to maintain the limit value.

The assumption of quasi-neutrality requires sheath models on the wall boundaries. In this simulation, the sheath edge, which means the boundary between the sheath and the pre-sheath region as shown in Fig. 2, corresponds to the computational boundary. One of the most important boundaries is the insert surface on which thermionic emission should be included into the sheath model. On this boundary, the following electron flux was assumed.

$$n_e \boldsymbol{u}_e \cdot \boldsymbol{n} = \frac{1}{4} n_e \sqrt{\frac{8kT_e}{\pi m_e}} \exp\left(-\frac{e\phi_{sh}}{kT_e}\right) - \frac{j_{em}}{e} \tag{5}$$

The first term in the right hand side is the electron loss from the bulk plasma, and the second term represents the contribution of the thermionic electrons which can be evaluated with Richardson-Dushman formula including Schottky effect,

$$j_{em} = AT_c^2 \exp\left(\frac{-e\phi_{eff}}{kT_c}\right), \quad \phi_{eff} = \phi_w - \sqrt{\frac{e|E_c|}{4\pi\varepsilon_0}} \tag{6}$$

where A, T_c and E_c represent Richardson-Dushman coefficient, insert temperature and electric field on the insert surface, respectively. Note that j_{em} is an absolute value of the emission current. The formula to evaluate E_c can be obtained by integrating Poisson equation (Gauss's law).[2] Since E_c depends on j_{em}, Eq. (6) should be iteratively solved with regard to j_{em}. The E_c also depends on the ion velocity at the sheath edge, where the ions were assumed to have Bohm velocity corrected due to the effect of thermionic emission.[15] Equation (5) is substituted into the electron flux of Eq. (3) on the insert boundary. On the cathode orifice boundary, we only have to vanish the second term of the right hand side of Eq. (5). The keeper electrode was assumed to be floated in accordance with the experiment,[16] i.e. the electron flux equal to the ion flux was assumed. On the plume boundary, in order to simulate discharge with a plate anode located downstream, the electric potential was set to a discharge voltage V_d at x/L_{em}=2.8, whereas V_d was periodically adjusted so that the discharge current can be kept around a specified value. On the other hand, no current condition was imposed on the upper boundary at y/L_{em}=0.8.

The electron thermal flux at the sheath edge of the insert surface can be evaluated as follows.

$$q_e = \frac{1}{4} n_e \sqrt{\frac{8kT_e}{\pi m_e}} \exp\left(-\frac{e\phi_{sh}}{kT_e}\right)(2kT_e + e\phi_{sh}) - \frac{j_{em}}{e}(2kT_c + e\phi_{sh}) \tag{7}$$

On the other wall boundaries, we can vanish the second term of the right hand side. On the inlet and plume boundaries, the electron temperature was fixed at assumed values.

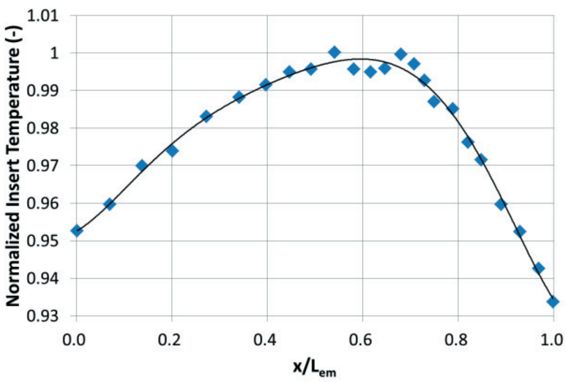

Fig. 1 Normalized insert temperature profile[10].

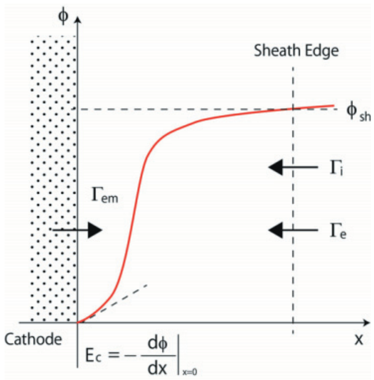

Fig. 2 Sheath with thermionic emission on insert surface.

D. Calculation Conditions

The calculation conditions are tabulated in Table 1. The working gas was Xe fed at a mass flow rate of 1 mg/s. The LaB_6 was selected as insert material and its maximum temperature $T_{c,max}$ was parametrically varied between 1850 and 1950 K for a constant discharge current of 30 A in order to understand qualitative influences of the insert temperature on the flow field. The keeper electrode was floated in accordance with the experiment condition at JPL. The inlet and outlet (plume boundary) electron temperatures, and the lower limit of the electron number density in the plume region were fixed at 1, 3 eV, and 5×10^{17} m^{-3}, respectively. The influence of these parameters on the results should be surveyed in the future.

Figure 3 shows the computational domain used in this simulation. In the Hybrid-PIC model, the mesh size should be equal to or less than the mean free path of the particle collisions. The minimum mesh size in the insert region used in the present study was set at 0.1 mm. This is much less than mean free paths with regard to the neutral-ion collisions including CEX. The shortest mean free path under consideration, however, is the Coulomb collision between ions, which is estimated in the order of 0.01 mm. The large mesh size may cause some numerical diffusion with regard to the ion's motion. Thus we should check the influence of the mesh size on the results in the future, even though the present mesh size is much less than the characteristic length in the insert region.

Table 1. Calculation Conditions

Gas	Xenon
Insert material	LaB_6 (A=29 A/cm^2/K^2, ϕ_w = 2.67 eV)
Mass flow rate	1 mg/s
Discharge current	30 A
Maximum insert temperature	1850 – 1950 K
Keeper condition	Floated
Inlet electron temperature	1 eV
Outlet electron temperature	3 eV
Lower limit of electron number density	5×10^{17} m^{-3}

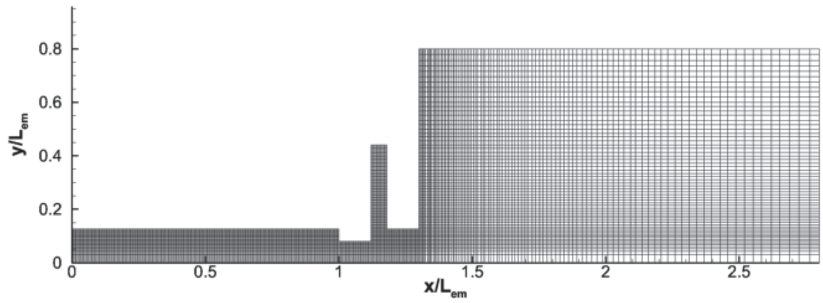

Fig. 3 Computational mesh.

III. Simulation Results

A. Discharge Field

Figure 4 shows the electron number density, electric potential, and electron temperature distributions for $T_{c,max}$=1900 K. The density has a peak about 7×10^{20} m^{-3} on the centerline around the middle of the insert region, and declines in the radial and axial direction. In the insert region, formation of the pre-sheath can be seen, which causes the radial plasma loss on the insert surface. The electric potential is increased from about 6 to 12 in the insert region, and then its gradient becomes higher around the orifice region. In the plume region, the density is nearly uniform at the specified limit value. The electric potential grows toward downstream region quite gradually and amounts to about 17 V in this case. The electron temperature behaves similar to the electric potential, where the temperature ranges from 1 eV to 2 eV in the insert region, and rapidly increases to about 3 eV through the orifice region, which corresponds to the specified value.

B. Influence of Insert Temperature

Figure 5 shows the electron density, electric potential, and electron temperature profiles along the centerline as a function of the maximum insert temperature $T_{c,max}$. We can see that the electron number density inside the cathode tube tends to be lower with higher $T_{c,max}$. While the top of the profile moves toward downstream direction as $T_{c,max}$ increases, the profiles overlap with each other in the range of $x/L_{em} > 1$, and the density approaches to the specified lower limit value in the end. Figure 6 shows comparison of the electron density inside the cathode tube between the simulation results and the experiment by JPL. This indicates that the simulation result for $T_{c,max}$ = 1900 K has most similar profile to the measured one in terms of not only qualitative but also quantitative aspect. The insert temperature of 1950 K seems unrealistic for the present conditions.

The electric potential profile inside and outside the cathode tube is significantly affected by the $T_{c,max}$. On the whole, the potential has positive gradient and the gradient becomes steep locally around the orifice region. The asymptotic values of the potential for $T_{c,max}$ = 1850 and 1900 K at the plume region are 20.5 and 16.1 V, respectively. Since the computational domain in the plume region is limited and we have no information about the anode sheath, fair comparison of the discharge voltage with the experiment is impossible, but these obtained values are not far from the measured value about 21 V for 30 A.[16]

The electron temperature profiles for $T_{c,max}$ = 1850 and 1900 K are nearly the same as a whole, whereas the line for 1850 K is slightly higher in the cathode tube. The profile for 1950 K has a undershoot in the cathode tube. This may be due to the excess energy loss on the insert wall caused by the low sheath potential, and the inappropriate electron temperature fixed at the inlet.

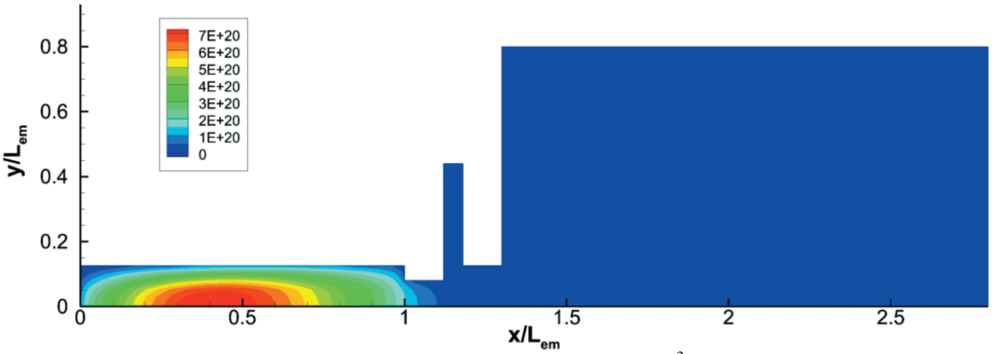

(a) Electron number density, m^{-3}

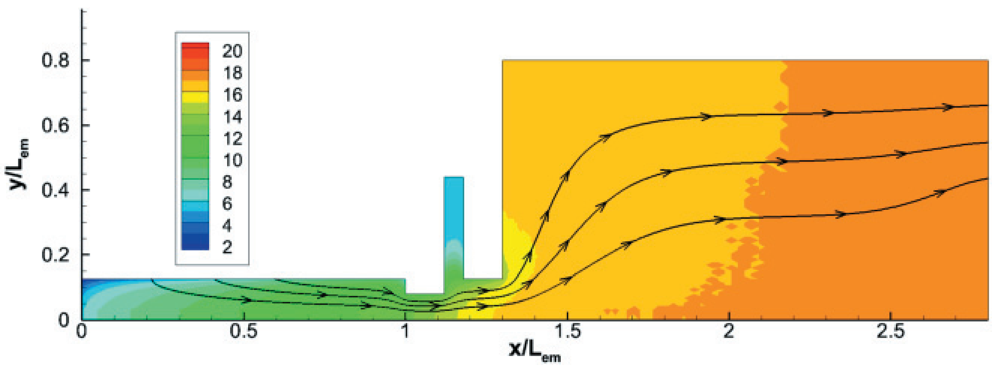

(b) Electric potential with electron streamlines, V

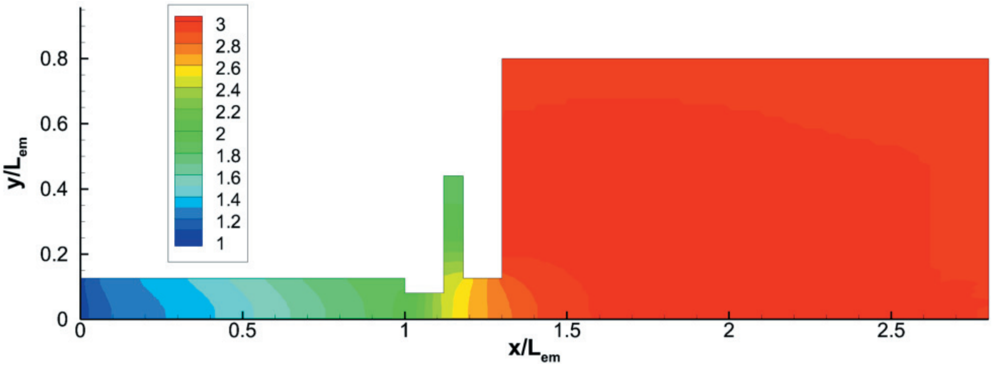

(c) Electron temperature, eV

Fig. 4 Flow field distributions for $T_{c,max}$=1900 K.

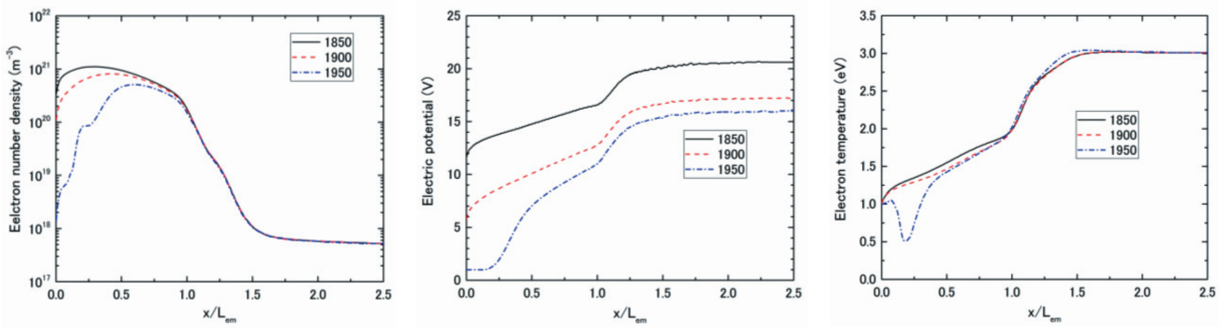

(a) Electron number density (b) Electric potential (c) Electron temperature

Fig. 5 Plasma characteristics along centerline for $T_{c,max}$ = 1850, 1900, 1950 K.

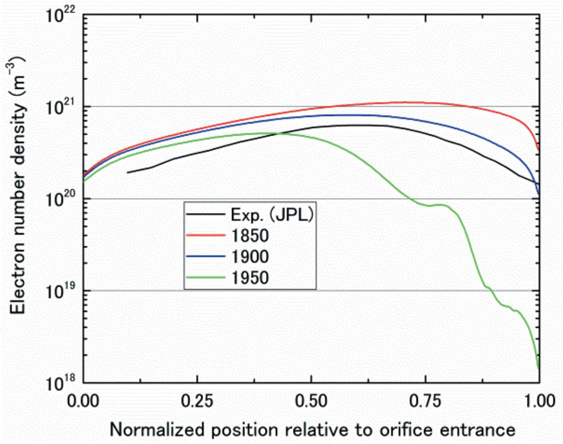

Fig. 6 Comparison of electron number density inside the cathode tube for $T_{c,max}$ = 1850, 1900, 1950 K between simulation and experiment by JPL[16].

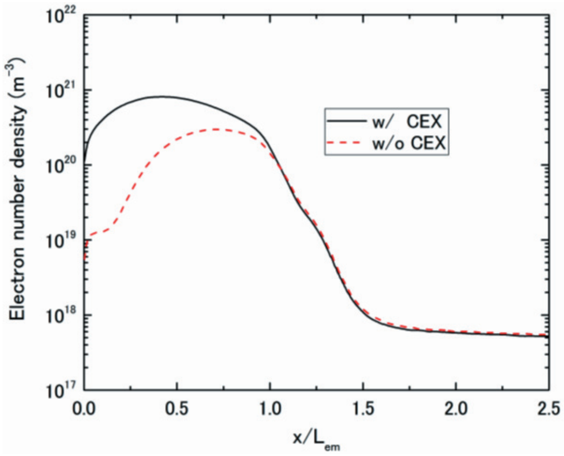

Fig. 7 Electron number density along centerline with and without CEX model for $T_{c,max}$=1900 K.

IV. Discussion

A. Electron Density Distribution

In Fig. 4-(a), the electron density has a peak around x/L_{em} = 0.4, which is consistent with the measured profile as seen from Fig. 6. The location of the density peak is affected by CEX collision. To clarify the role of the CEX collision in the flow field, the electron density profiles with and without CEX collision are compared in **Fig. 7**. We can see that, if CEX is ignored, the peak location shifts downstream, which is attributed to the heavy particle's behavior. Figure 8 shows the streamlines of neutrals and ions inside the cathode tube with and without CEX. Without CEX, the neutrals have basically positive velocity in x direction. The streamlines extended from the insert surface is due to the neutrals produced by recombination, i.e. ions are attracted to the insert surface by the potential gradient in the pre-sheath, and turn into neutrals via recombination with electrons. On the other hand, when CEX is considered, the streamlines of neutrals are folded back, which generates the vortex near the inlet. This is because the neutrals initially flowing downstream are supposed to be replaced with ions flowing upstream by CEX collisions, then the new neutrals tend to be directed in –x direction especially near the centerline where the ion density is relatively high. This mechanism plays a role in rising neutral density near the inlet, which contributes to increasing ion/electron density and consequently to the shift of the density peak location.

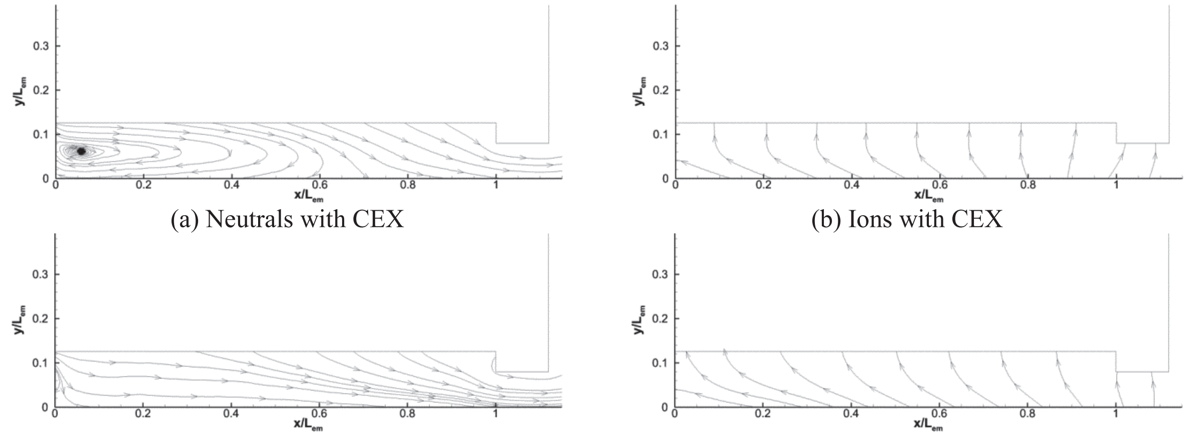

(a) Neutrals with CEX (b) Ions with CEX

(c) Neutrals without CEX (d) Ions without CEX

Fig. 8 Streamlines of neutrals and ions with and without CEX model for $T_{c,max}$=1900 K.

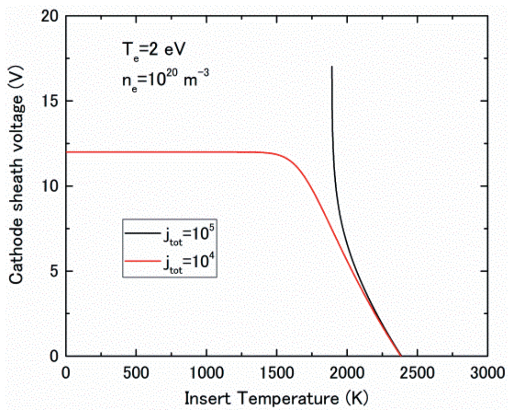

Fig. 9 Relation between cathode sheath voltage and cathode temperature: *The ion velocity is assumed to be standard Bohm velocity, and Schottky effect is ignored.*

B. Influence of Insert Temperature

To clarify why the electron number density inside the cathode tube tends to be lower with higher $T_{c,max}$, loss of the electrons is discussed in terms of the electric potential. The electric potential inside the cathode tube is basically sustained by the electron-repelling sheath formed on the insert surface. The influence of the insert temperature on the sheath voltage can be qualitatively understood from the equation of current conservation at the sheath edge.

$$j_{tot} = j_i - j_e + j_{em} = j_i - j_{th} \exp\left(-\frac{e\phi_{sh}}{kT_e}\right) + j_{em} \rightarrow \phi_{sh} = -\frac{kT_e}{e} \ln\left(\frac{j_i - j_{tot} + j_{em}}{j_{th}}\right) \tag{8}$$

$$\text{where} \quad j_{th} = \frac{1}{4} e n_e \sqrt{\frac{8kT_e}{\pi m_e}}$$

Here j_{tot}, j_i, j_e, and j_{em} are a total current, ion current, plasma electron current, and emission current, respectively. Note that each current denotes an absolute value. If the ion velocity at the sheath edge toward the wall is assumed to be the standard Bohm velocity ($=\sqrt{kT_e/m_i}$), and the Schottky effect is ignored, the sheath voltage can be calculated from Eq. (8) as a function of the insert temperature for constant j_{tot}, n_e and T_e. When $n_e = 10^{20}$ m^{-3} and $T_e = 2$ eV, the relation between the sheath voltage and the insert temperature for $j_{tot} = 10^4$ and 10^5 A/m^2 can be depicted like in Fig. 9. Depending on j_{tot}, the ϕ_{sh} takes on quite different characteristics. This can be understood from Eq. (8), i.e. when $j_{tot} < j_i$, the ϕ_{sh} can be kept finite even at a low insert temperature, but otherwise, the ϕ_{sh} is to diverge at a certain cathode temperature. From these curves, we can presume the ϕ_{sh} tends to be higher with lower insert temperature regardless of j_{tot} around $T_c = 1900$ K. This is why the electric potential becomes higher with lower insert temperature as seen in Fig. 5-(b).

The higher sheath potential on the insert will repel more electrons, which leads to suppression of electron's thermal loss into the wall surface. This causes the tendency of the electron temperature inside the cathode tube as seen in Fig. 5-(c). The higher electron temperature results in large ionization rate, thus the electron density for lower insert temperature becomes higher. Since the initial energy of an ion produced in the insert region is the same as the original neutral's one, the ion are pushed back upstream due to the electric potential and tends to be accumulated inside the tube.

V. Conclusion

The plasma flow of the hollow cathode was simulated with the newly developed Hybrid-PIC code which models ions and electrons as particles and fluid, respectively. In this study, the applicability of the model for the hollow cathode was demonstrated, and the influences of the insert temperature on the flow field were discussed under a constant discharge current of 30 A and a mass flow rate of 1 mg/s as a first step. The insert temperature T_c was parametrically varied from 1850 to 1950 K. The inner diameter and the length of the insert were set to the same as those of 1.5 cm class cathode of JPL, which enables us to compare our results to the available experimental data.

The comparison with the experimental data shows that the electron density profile in the insert region for T_c = 1900 K agrees well with the measured data, which suggests the applicability of the model to the hollow cathode plasma. As the insert temperature decreases, the electric potential becomes higher, and then the electron energy loss through the electron repelling sheath is suppressed, which leads to the higher electron temperature, and hence higher electron number density. It was also found that CEX collision makes the neutrals pushed back toward upstream in the middle of the cathode tube, which strongly affects the electron density profile.

Acknowledgments

This research has been supported by a Grant-in-Aid for Scientific Research (B) (26820377) from the Japan Society for Promotion of Science.

References

[1]Goebel, D. M., Jameson, K. K., Watkins, R. M., Katz, I., and Mikellides, I. G., "Hollow cathode theory and experiment. I. Plasma characterization using fast miniature scanning probes," *Journal of Applied Physics*, Vol. 98, 113302, 2005.

[2]Mikellides, I. G., Katz, I., Goebel, D. M., and Polk, J. E., "Hollow cathode theory and experiment. II. A two-dimensional theoretical model of the emitter region," *Journal of Applied Physics*, Vol. 98, 113303, 2005.

[3]Coletti, M., and Gabriel, S. B., "Insert Temperature Measurements of a 180A Hollow Cathode for the HiPER Project," AIAA-2012-4081, 2012.

[4]Thomas, R. E., Kamhawi, H., and Williams, G. J., "High Current Hollow Cathode Plasma Plume Measurements," IEPC-2013-076, 2013.

[5]Katz, I., Mikellides, I. G., Goebel, D. M., and Polk, J. E., "Plasma Heating of Inert Gas Hollow Cathode Inserts," IEPC-2007-017, 2007.

[6]Goebel, D. M., Jameson, K., Katz, I., and Mikellides I. G., "Energetic Ion Production and Keeper Erosion in Hollow Cathode Discharges," IEPC-2005-266, 2005.

[7]Jorns, B. A., Mikellides, I. G., and Goebel, D. M., "Temporal Fluctuations in a 100-A LaB6 Hollow Cathode," IEPC-2013-385, 2013.

[8]Parra, F. I., Ahedo, E., Fife, J. M., and Martínez-Sánchez, M., "A two-dimensional hybrid model of the Hall thruster discharge," *Journal of Applied Physics*, Vol. 100, 023304, 2006.

[9]Nanbu, K., Kitatani, Y., "An ion-neutral species collision model for particle simulation of glow discharge," *Journal of Physics D*, Vol 28, 1995, pp.324-330.

[10]Mikellides, I. G., Goebel, D. M., Jorns, B. A., Polk, J. E., and Guerrero, P., "Numerical Simulations of the Partially-ionized Gas in a 100-A LaB6 Hollow Cathode," IEPC-2013-142, 2013.

[11]Goebel, D. M., and Katz, I., *Fundamentals of Electric Propulsion: Ion and Hall Thrusters*, John Wiley & Sons, Inc., New Jersey, 2008.

[12]Amestoy, P. R., Duff, I. S., Koster, J., and L'Excellent, J. Y., "A fully asynchronous multifrontal solver using distributed dynamic scheduling," *Journal of Matrix Analysis and Applications*, Vol. 23, No. 1, 2001, pp. 15-41.

[13]Goebel, D. M., Watkins, R. M., and Jameson, K. K., "LaB_6 Hollow Cathodes for Ion and Hall Thrusters," *Journal of Propulsion and Power*, Vol. 23, No. 3, 2007, pp. 552-558.

[14]Jameson, K. K., Goebel, D. M., Mikellides, I., and Watkins, R. M., "Local Neutral Density and Plasma ParameterMeasurements in a Hollow Cathode Plume," AIAA-2006-4490, 2006.

[15]Prewett, P. D., and Allen, J. E., "The double sheath associated with a hot cathode," *Proceedings of Royal Society of London*, Vol. 348, 1976, pp. 435-446.

[16]Goebel, D. M., and Chu, E., "High Current Lanthanum Hexaboride Hollow Cathodes for High Power Hall Thrusters," IEPC-2011-053, 2011.